

# Structural characterisation of rock mass defects: a comparison of traditional and emerging technologies

S. Fityus / K. Thoeni

*The University of Newcastle, Callaghan, Australia, Stephen.fityus@newcastle.edu.au*

J. Cudmore, A. Giacomini

*The University of Newcastle, Callaghan, Australia*

**ABSTRACT:** Emerging technologies are revolutionising the way in which rock mass defects are being characterised. The traditional approach of measuring rock discontinuities using a geological compass is being replaced, both by alternative direct-contact measurement devices as smartphones with applications that directly give dip and dip direction, and by low-cost non-contact approaches such as photogrammetry performed on digital images to develop a 3D model of the rock face, thereby allowing virtual measurements of discontinuities to be taken. This paper presents a comparison of the accuracy of these different approaches to gathering orientation data (dip angle and dip direction) for discontinuities in natural rock masses, with accompanying consideration of the efficiency and relative cost of various contact and non-contact methods. Two mobile phones with different apps were used to take contact measurements and several different cost/quality image sensors were used to capture digital images for the photogrammetric models. Several image sets were collected and subsequently processed using Agisoft Metashape to develop 3D point clouds and eventually a high-resolution 3D model. The open-source package CloudCompare was used to virtually take measurements of the features. The average of conventional geological compass measurements was used as a benchmark. From the results, most of the methods were generally found to be acceptably reliable. Of the results from the smartphone applications, that of the iPhone 4 (an older generation) was more unreliable. It provided inaccurate dip direction due to the device constantly requiring calibration. Generally, the dip angle was approximated better than the dip direction for both devices. The photogrammetric models provided results closest to the compass from the highest quality sensor as expected. All models performed relatively well, the dip angle was close to the compass for most approaches, and the dip direction provided least error on the higher accuracy approaches.

**Keywords:** geostructural mapping, low-cost sensors, photogrammetry, point cloud, smartphone

## 1. Introduction

Discontinuities, “geostructural features” or “rock defects” are general terms used to describe a variety of features of rock masses. These rock features can have adverse effects on the engineering behaviour of rock masses, such as reduction in strength, increase in deformability and anisotropic permeability. Failure in a rock mass will usually occur within or involve these defects, where they exist.

Geostructural features in rock masses include bedding surfaces, foliations, joints and faults (Figure 1). They include both actual defects as well as structures and fabrics which represent potential defects. On a small scale (at least), these features usually present approximately planar surfaces, the orientation of which can be characterised by a set of angular measurements such as dip direction, dip angle and strike, as defined in Figure 2.

The dip angle is the steepest inclination of the structural feature plane, relative to the horizontal plane, as shown in green on Figure 2. Therefore, by definition, the dip angle must be between zero (perfectly horizontal) and ninety (vertical) degrees. The dip direction is the declination angle from north to the projection of the dip angle vector into the horizontal plane. The dip direction is usually defined by a full circle angle between zero to three hundred and sixty degrees.

The traditional method of obtaining geostructural data is a geological compass. The modern geological compass has been in use for around 70 years, however the concept is based on magnetic compasses which have been in use since the 11th century [1]. Major issues with manual field data collection include safety, accessibility, human error and time.



**Figure 1.** Geostructural features: bedding (top left); foliation (top right); joints (bottom left) and faults (bottom right).

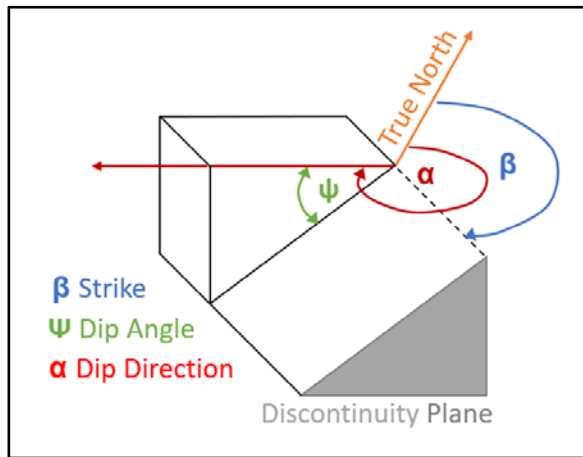


**Figure 2.** Geostructural feature orientation definitions.

It has only been with recent technological advances that devices like smartphones have been able to make use of built-in sensors such as accelerometer, gyroscope and compass via applications to measure discontinuities [2-7]. This has created opportunity for potentially more efficient methods of obtaining geostructural information. Compared to a geological compass that gives only raw data and generally requires software to plot the data, the phone applications can measure the orientation of features and then present a plot of the data collected. Streamlining of the process is the main allure of the use of smartphones in measuring the attitude of geostructural features. The purpose of using virtual compasses in the form of phone applications is mainly the ease of use and convenience. Taking measurements using traditional methods like the geological compass is often difficult and time consuming [5].

Proximity remote sensing methods such as photogrammetry and terrestrial laser scanning (TLS) are alternatives that provide new avenues of data collection and analysis [8-15]. These methods allow to gather a large amount of data in the form of 3D point clouds (and/or 3D surface models) of rock mass exposures, from which virtual measurements can be taken. Whereas a laser scanner samples millions of points to create a dense 3D point cloud of its own, the collected digital images need to be post-processed using for example SfM-MVS software. The latter can be computationally very demanding. However, recent advances in computer vision and increasing processing power have facilitated a new era of 3D mapping. In addition, the power of photogrammetry has been strengthened by the deployment of sensors using complementary technologies such as unmanned aerial vehicles (UAVs) [16-20].

These proximity remote sensing methods provide added benefits such as keeping the user safe and providing more data in an automated way. The advancements in clever and efficient TLS technologies over the last 15-20 years might have discouraged the development of other techniques such as photogrammetry, however with growing computational power and the development of new low-cost sensors it has been quite the opposite [21-23].

This paper compares and evaluates some of these emerging technologies by conducting a systematic analysis of measurements taken at a rock face.

## 2. Scope

For this study, a variety of different technologies were used to obtain geostructural data, and this was compared with the data for the same geostructural surfaces measured using a geological compass as the benchmark. A Freiburger geological compass (Figure 3) was used to produce the benchmark measurements for this study.

The new technologies for geostructural feature measurement include both devices which act as direct alternatives to compasses, and which measure through direct contact with rock, and technologies which can produce virtual 3D models of rock exposures, from which measurements can be taken.

Whilst accuracy is the primary consideration, the cost and efficiency of the technology was also considered. Measurements of designated rock surface features were taken which included the dip angle and dip direction, with the strike also found by subtracting 90° from the dip direction. The accuracy of measurements is evaluated by determining the absolute error produced from subtracting the various method measurements from an average compass measurement.



**Figure 3.** Freiburger geological compass.

## 3. Technologies studied

The technologies used in this study fall into two main categories: contact-based technologies, which comprise devices that are effectively alternatives to the traditional geological compass and which must be placed on the subject surface to obtain a measurement; and non-contact technologies, which are devices that can scan and measure a rock exposure remotely to create a 3D virtual model (point cloud and/or mesh), from which measurements of the surface can be recreated and geostructural data extracted. A wide variety of technologies was selected ranging in quality and price.

### 3.1. Contact Technologies

The contact technologies included in this study were all smartphones, employing applications allowing them to be used as a geological compass through data provided by the built-in sensors that are available on many smartphones these days. Smartphones require compass and inclinometer sensors to utilise geological compass applications. The compass sensor acts the same as a magnetic compass and is used to measure orientation of the phone. The inclinometer sensor is used to measure the inclination of the smartphone at any given time. Whereas

inclinometer sensors are very common and present in almost every smartphone, this is not the case for the compass sensor.

Smartphone geological compass applications provide an array of features and benefits such as ease of use and accessibility. They also streamline the tasks, can store the measurements to a file and even plot the measurements stereographically on the go.

For this study an Android Oppo R9 phone and an Apple iPhone 4 were considered and used in conjunction with varying compass applications (Figure 4). For the Android Oppo R9, the Geological Compass (GC) free from the Android store was used. The eGEO Compass Pro was also considered but it is not free and initial tests showed that it is giving the same results as the GC free. For the apple iPhone 4, the Lambert app from the Apple store was used.

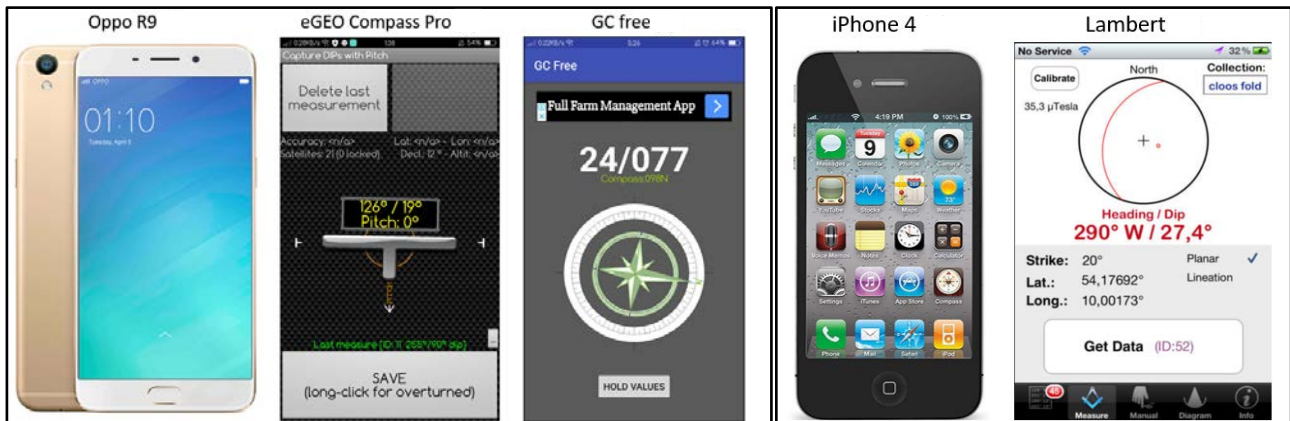


**Figure 4.** Oppo Android phone (image from productreview.com.au) with applications (left) and Apple iPhone (image from amazon.com) with application (right).

### 3.2. Non-Contact Technologies

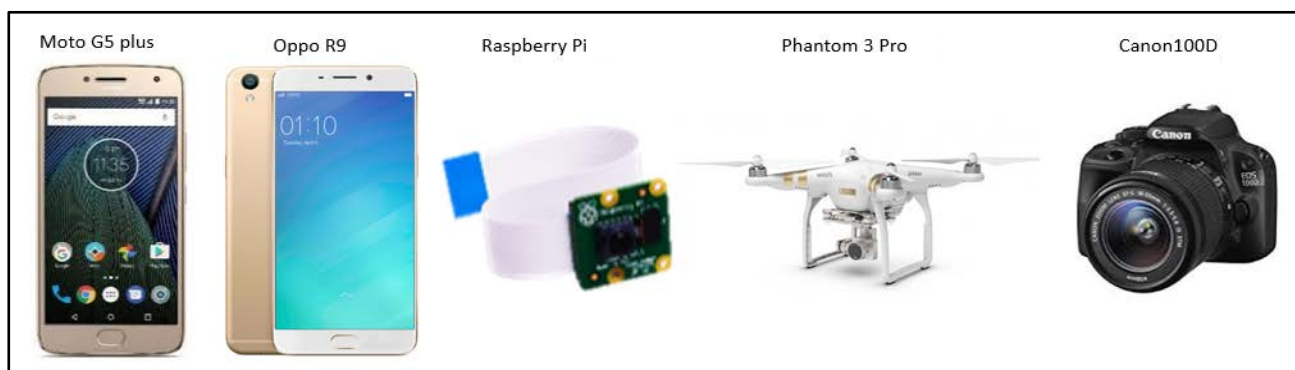
Non-contact technologies are also commonly referred to as ‘remote sensing’ technologies. For this study, the technologies chosen all work by utilising a photographic sensor within a device to capture photographic digital images. These are then processed using a software which creates a high-resolution 3D model (dens point cloud and mesh) of the rock face/exposure. The geostructural characteristics of any facet of the modelled surface can then be extracted, either manually or automatically.

A variety of different devices from very low cost to professional grade cameras were used to acquire imagery for this study to compare how their properties affect the result and to see whether simple everyday cameras can produce reliable information. Figure 5 shows the different contact-less devices used in this study, which include two smartphones (Moto G5 plus and Oppo R9), a Raspberry Pi with a camera module, a Phantom 3 Pro UAV with inbuilt camera and a Canon 100D DSLR camera.

They were selected for their variety in cost and resolution. Low-cost cameras generally have smaller sensors and less stable optics when compared to higher cost cameras like DSLR.

Shown in Figure 6 is a diagram of how a camera takes an image. What the sensor actually acquires in a 2D image, and its resolution, depends upon a combination of the physical size of the sensor (width in mm), the object distance (mm) and the focal length (mm). The sensor captures information pixel by pixel, where the width of a pixel (mm) is the sensor width divided by the number of pixels. The corresponding size of the view that is captured by each pixel is known as the Ground Sampling Distance (GSD, in mm per pixel) which determines the size of one pixel in the field. The accuracy of the final 3D model is directly affected by the resolution and quality of the image sensor and its optics [23].

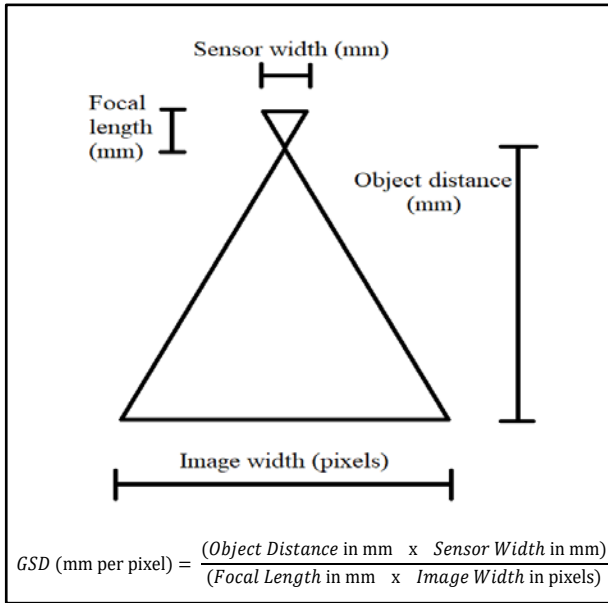
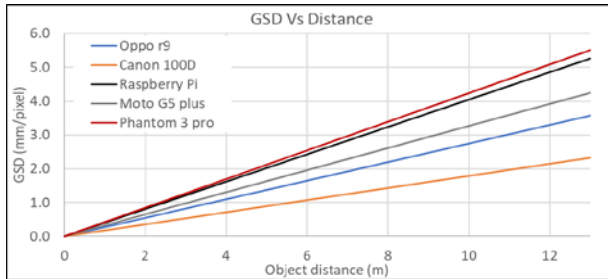
Listed in Table 1 are the properties of each of the camera sensors used as contact-less devices for this comparison study. They were obtained from the manufacturer’s specifications.



**Figure 5.** Non-Contact (photographic sensors) used in this study (images from: productreview.com.au, amazon.com, bhphotovideo.com).

**Table 1.** Properties of each of the camera sensors used as non-contact devices for this comparison study

Sensor model	Resolution MP	Resolution pixels	Sensor type -	Sensor size mm	Pixel size μm	Focal length mm	Focal length pixels
Canon 100D	18	5184x3456	CMOS	22.3x14.9	4.38	24	5738.88
Moto G5 plus	12.2	4032x3024	CMOS	5.65x4.24	1.4	4.28	3059.04
Raspberry pi	8	3280x2464	CMOS	3.68x2.76	1.12	3.04	2580.03
Oppo R9 (and GPS)	12.98	4160x3120	CMOS	4.69x3.52	1.127	3.5	3143.38
Phantom 3 Pro (and GPS)	12	4000x3000	CMOS	6.30x4.72	1.56	3.61	2322.29

**Figure 6.** Relationship between the GSD and the sensor width.**Figure 7.** Relationship between GSD and the object distance for various camera sensors.

From the data in Table 1, and the geometry of Figure 6, the relationship between GSD and object distance was determined for each sensor, as shown in Figure 7. This was utilised in determining a suitable distance from the studied rock surface to take photographs used for the geostructural analysis.

The acquired digital images were processed to produce dense 3D point clouds from which measurements of geostructural data were taken. The software used for this process was Agisoft Metashape [24]. This software utilises SfM-MVS to process 2D digital images to obtain 3D information. In comparison to traditional optical surveying techniques, SfM-MVS is much faster and cheaper in terms of data acquisition [10].

A complication arising from the low-cost non-contact technologies that employ photogrammetric surface modelling is that the digital surfaces created are generally not explicitly referenced in space (unless built-in GPS data is available), so that absolute geostructural data cannot be directly extracted. To obtain meaningful geostructural data, the models produced via photogrammetry must be georeferenced. This was achieved using ground control points (GCP) which were measured using a total station. The use of the total stations allows for accurate 3D positioning of points on a rock mass surface to the nearest millimetre. The GCP were then selected on the images before processing the image sets with the SfM-MVS software to obtain the virtual models. The virtual models were then exported and inspected using the open-source tool CloudCompare [25].

The GPS models use the GPS coordinates stored from the image set (geographic coordinates of the built-in GPS antenna at the time of the image acquisition are recorded in the EXIF metadata of the image) taken as a georeference rather than the GCP in the images. This exercise was performed to get an idea how accurate measurements from models georeferenced using standard built-in GPS could be, knowing that the accuracy of the built-in GPS is rather low (generally in the range of 5-10 m).

#### 4. Study Site

The site chosen for this study was Pilkington Street Reserve, North Lambton, NSW, Australia. The site is a disused quarry which formerly produced blocks of the Permian Waratah Sandstone, a very-thickly bedded, massive, medium-grained, lithic sandstone. This site has since been rehabilitated and is now used as a recreational area. Images of the site are shown in Figure 8.

The specific area worked on for measurements is illustrated from A-A to B-B in Figure 8. The width of the rock mass studied was around 25-30 m and the average height was around 6 m. The rock mass investigated is characterised by widely-spaced, joints that are mostly planar and smooth, which form the majority of exposed surfaces. There are two perpendicular, persistent, primary joint sets as well as some non-persistent joints and some quarry-induced fractures. These afforded a good variety of sloping surfaces in many directions to serve as places for measurement. There is a small retaining wall built on the top portion and there is some significant grassy vegetation around the rock face and a few trees on top, to the right.



(a) General view of Pilkington Street Reserve, North Lambton, NSW.



(b) Specific measurement area.

**Figure 8** Images of the studied rock faces at the study site.

## 5. Methodology

### 5.1. Fieldwork

A set of GCP were established on the site for accurate georeferencing of the photogrammetric models. These were positioned to be clearly visible points that were easy to find. GCP typically are coded targets or natural features, depending on accessibility [19]. For the purpose of this paper, an intermediate method was used. Chalk targets ( $10 \times 10$  cm square) were drawn on selected features of the rock face, as shown in Figure 9. The inner corners of the square were used as GCP.

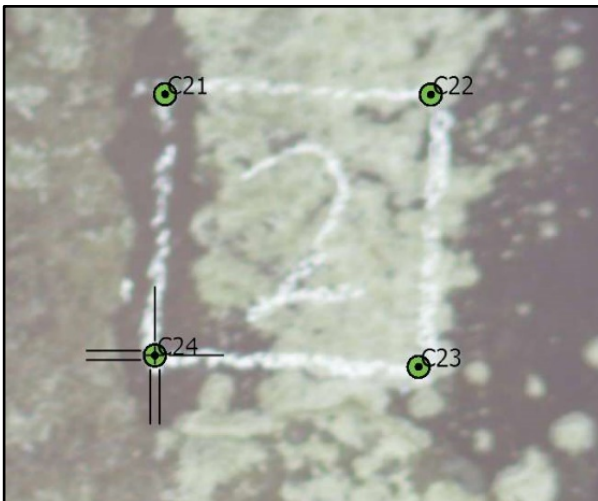


**Figure 9** Set of Ground Control Points (GCP). The four inner corners of the square where measured and used as GCP.

The coordinates of the GCP were measured using a total station set up at a distance of approximately 20 m of the centre of the rock face. Measurements were taken to the coordinates of the four corners of the square. The accuracy of the coordinates of the GCP and check points should ideally be smaller than that of the GSD [23]. Due to the high accuracy of the total station and the rather close set up this was easily achieved.

Due to the positioning of the rock face, the optimum time for lighting is in the afternoon. This is when the least amount of shadow is on the rock face, with the sun shining directly on the face. This meant that the photogrammetry data collection would be completed late in the afternoon.

The image footprint was selected to achieve an image overlap of about 80% since an overlap of 60-80% is recommended as a basis for good quality models [10].

#### 5.1.1. Contact Data Acquisition

Locations were selected for the contact measurement points. At each location, a  $10 \times 10$  cm flat plywood block was placed on the rock face in the general position to take the measurements. The block was translated and rotated until it sat firmly and relatively flat on the rock face, then chalk was used to mark a square around the block. The block was taken off and a point number was written in the centre of the square to identify the point of measurement. The marked squares were the same one as the used for the GCP (see Figure 9).

Two sets of contact measurements were made; one set with the block in place as a base for the device, and the second with the device resting directly on the rock. Firstly, the android application Geological Compass free was used through the Oppo phone orientated in both portrait and landscape orientations. The phone was placed in the centre of the block, the application was opened on the phone and the dip angle and dip direction were written down on a data sheet. This same process was applied to the apple application Lambert via the iPhone 4. This is shown in Figure 10. After this the geological compass was used to measure the dip direction and angle.



Figure 10 Contact measurement with block.

Once the measurements from the applications and the compass were taken, the 10 × 10 cm block was removed from the surface and the same measurements were taken directly on the rock surface within the marked square. Figure 11 shows examples of the measurements without the block on the surface. The same notation was used for the corresponding devices with a \* at the end, for example the Oppo portrait measurement was called “OP\*”.

This process was repeated for 22 points at the base of the rock face, then 5 points at the top of the rock face with the final 3 points on the retaining wall above the rock face making a total of 30 points.



Figure 11 Contact measurement capture modes.

## 5.1.2. Non-Contact Data Acquisition

Using the charts previously discussed in Figure 7, the lowest possible GSD was selected that allowed a reasonable object distance to minimise the number of photos needed to capture the whole rock face. A GSD of 2-3 mm/pixel was chosen. Once all image footprints were determined for the chosen GSD, the object distances were physically marked out in front of the rock face, maintaining approximately the same distance from the irregular rock face along its length.

For the required image overlap of 80%, the distance between each photo was roughly 1 m between photos for all the models.

## 5.2. Data Analysis

### 5.2.1. Processing of Digital Images

The commercial program Agisoft Metashape Professional [24] (previously known as Agisoft Photoscan) was used to process the digital images into 3D models (dens point clouds and meshes). The same processing parameters as in Thoeni et al. [23] were used for all models. Table 2 summarises information relating to each non-contact sensor and the data acquired.

Table 2. Contact-less Data Statistics.

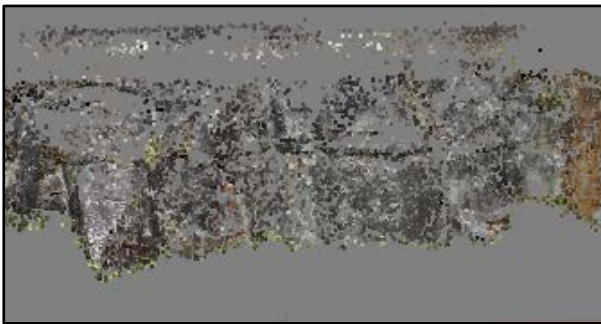
Sensor model	GCP #	Images #	Object Distance m	GSD mm/pixel	Coverage Area m <sup>2</sup>
Canon 100D	100	46	14.5	2.52	82.9
Moto G5 plus	100	60	7.8	2.57	93.9
Rasp. Pi	100	68	7.7	2.99	110
Oppo R9	100	60	9.7	3.1	102
Phantom 3 Pro	104	73	7.8	3.34	122
Oppo R9 GPS	0	60	9.7	3.1	102
Phantom 3 Pro GPS	0	73	7.3	2.93	242

Image processing to build rock surface models involves a series of steps [23]. Image masking is first performed to remove sections of foliage. This only left the rock face fully visible to be used in the model. An example of an image with the foliage masked is shown in Figure 12.



**Figure 12.** Example of image masking in Metashape.

Once all the image masks were created, photo alignment was carried out in preparation to build a sparse point cloud. The program identifies the position and orientation of the camera, for each of the photos imported into the project. Two sparse clouds were generated for each model at high resolution. Shown in Figure 13 is a portion of the initial sparse point cloud generated for the Moto G5 plus after the alignment process.



**Figure 13.** Typical initial sparse point cloud.

The coordinates of the GCP were imported into Metashape to georeference and constrain the 3D model. During the field work photos were taken of each measurement point with the GCP marked on them, these were used to cross reference the image in the sparse point cloud with the survey data. For each GCP, an image containing that point was identified within the data set of the sparse point cloud. Once it was found, the four markers were placed on the four inner corners. This was repeated for two images in the data set, after which the software located other photos with the same point.

Filtering the photos to show only the images with the measurement sites after they had been selected on the image pairs allowed them to then be corrected and in turn, un-corrected ones were adjusted by the software and made slightly more accurate.

It took around 4 hours to mark all GCP correctly for each model; in all, 120 GCP were manually located on as many as 60 images for each model. It should be noted that generally only 3 GCP are needed for georeferencing but additional GCP improve the accuracy of the model, especially because they can be used as external constraints in the bundle adjustment [23]. Hence, although

generally not practical, all GCP were used to get the best accuracy. This is seen as an academic exercise. A more practical relevant scenario would be the use of coded targets and minimise the number of GCP needed for accurate georeferencing.

Generally, after processing the sparse point cloud, the point cloud was cleaned of any noticeably incorrect points. Scattered points (outliers) that clearly were not part of the desired model were removed manually. In addition, points with a high reprojection error were gradually selected and removed. The latter improves the overall accuracy of the model [23].

A dense point cloud of high quality was then generated for each sparse point cloud. Each model took between 19 and 37 minutes to calculate, generally turning the sparse point cloud of ~30,000 points into a dense point cloud of ~10 million points. Shown on Figure 14 is part of the dense point cloud produced from the Canon 100D after it has been cleaned up.

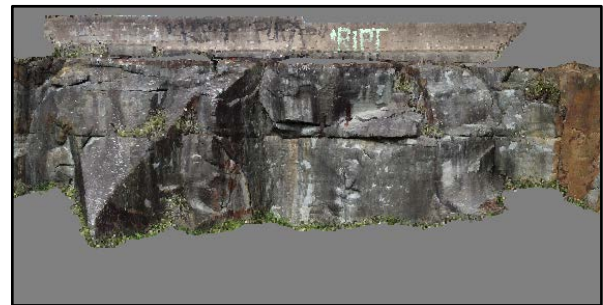


**Figure 14.** Typical dense point cloud.

### 5.2.2. Measurements on Digital Models

Measurements of dip and dip direction from the photogrammetric models were made at the marked locations on the rock face using the Compass plugin tool [14] in CloudCompare which involved fitting the diameter of a circle to pass through the points on the corners of the marked square on the rock face, as is shown on Figure 15a. The software then finds a plane that best fits the points within the circle (Figure 15b).

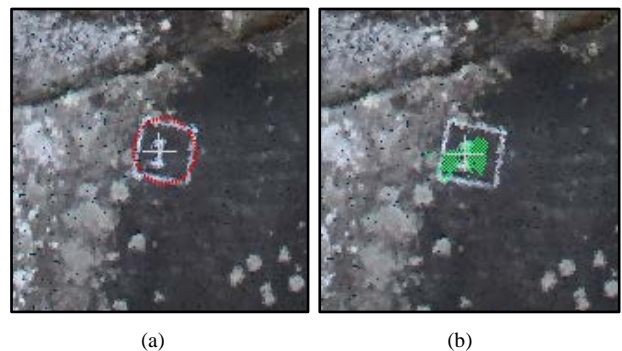


**Figure 15.** Selection of region (a) and fitting of a plane (b) in CloudCompare using the Compass plugin.

## 6. Results and Discussion

In the results that follow, Table 3 explains the codes to identify the various results.

**Table 3.** Codes used in the presentation of results.

Technology	Code	Category	Set	Coverage Area
Freiberger Compass	-	contact		Block
			*	Rock
Lambert app on iPhone 4	I	contact	IP	Block, portrait
			IP*	Rock, portrait
			IL	Block, landscape
			IL*	Rock, landscape
GC free app on Oppo R9	O	contact	OP	Block, portrait
			OP*	Rock, portrait
			OL	Block, landscape
			OL*	Rock, landscape
Canon 100D	C1	non-contact	C1	3D model
Moto G5 plus	M1	non-contact	M1	3D model
Raspberry Pi	R1	non-contact	R1	3D model
Oppo R9	O1	non-contact	O1	3D model
Phantom 3 Pro	P1	non-contact	P1	3D model
Oppo R9 GPS	OG1	non-contact	OG1	3D model
Phantom 3 Pro GPS	PG1	non-contact	PG1	3D model

In evaluating the different measurement technologies, it is assumed here that the measurements made using the conventional Freiburger compass are correct, and the performance of the different technologies is based upon how well their measurements compare with the compass measurements, for the 30 different surfaces measured.

For each of the different technologies trialled, a set of results like the ones in Figure 16 were generated. It is apparent from Figure 16 that the 39 surfaces captured in the study included a diverse range of dip angles (almost flat to vertical), but a less diverse range of dip directions, being somewhat biased by the exposures available in a localised exposed rock face.

Figure 16 shows the results for the GC free app on the Oppo R9 device. Figures 16a-b indicate that the error in this measurement technique is relatively small and randomly scattered on either side of the compass value. Greater detail on the absolute error is given by Figures 16c-f, which suggest that there may be a slightly greater tendency to overestimate both the dip and dip direction with this approach. The error in dip angle is generally less than 2 degrees but may be as big as 7 degrees. The error in dip direction is generally less than 10 degrees but may be up to 20 degrees.

The results of Figure 16 also suggest that the error in the dip angle is not affected by whether the device is oriented in portrait or landscape on the face, or whether it is placed on a backing block, or directly against the rock. The error in dip direction is also unaffected by the use of a mounting block, but it does seem that the error is reduced when the device is oriented in landscape position; this seems to reduce the incidence of errors

exceeding 10 degrees. The same information is also captured in Table 4.

Table 5 presents the data of Table 4, for all of the tested technologies, compiled for comparison. In general, there is not much difference between the available technologies, and certainly, the performance is not directly proportional to price. Both contact and non-contact technologies appear to be capable of giving reliable measurements of dip and dip direction in most situations. There is no case to argue that contact technologies are more or less reliable than non-contact technologies.

Of the two contact methods considered, the GC free app on the Oppo R9 smartphone did clearly outperform the Lambert app on the apple iPhone, with similar abilities to reliably determine dip angle, but a much lower likelihood of returning an error in dip direction in excess of 10 degrees.

Of the different non-contact approaches, all but the model derived from the Oppo R9 images gave similarly reliable values of dip and dip direction. Data derived from the Oppo R9 images had a significantly higher likelihood of being in error by more than 10 degrees. This might indicate that the image sensor is of less quality than the one for the other sensors. A standout in relative performance was the model derived from the Raspberry Pi camera module, which supported values as reliable as those derived from images captured by the much more expensive Canon 100D or Phantom 3 Pro.

To provide some additional sense of overall performance, Figure 17 shows a comparison of results for two different measurement points (i.e. locations marked out on the rock face): Point 2 which gave relatively consistent values of dip and dip direction for all of the different technologies, and Point 16, which displayed relatively greater variability. For Point 2, both dip and dip direction fall within 2 degrees of the benchmark values, except for the GC free app which underestimates the dip direction by 8 degrees. For Point 16, the contact methods generally overestimate the dip and the non-contact generally underestimate, but in each case by not more than 1 or 2 degrees. The dip direction, however, is overestimated by the iPhone by more than 30 degrees, and underestimated by the model derived from the Oppo G9 images by 20 degrees (due to a noisy point cloud). The inaccuracy of the iPhone measurement might be related to some calibration issues, whereas the one of the Oppo G9 is related to some noise in the 3D model.

Table 5 also summarises the cost and time for each sensor. It should be noted that for the contact measurements the time refers to the time spend on the site to conduct the actual measurements. It should also be noted that more than one measurement per location was carried out. For the non-contact technologies, the time refers to the total time including capturing of images, processing and taking the measurements on the virtual models. It should be noted that the time also includes the time to select all GCP (about 4 hours), except for the one with GPS, which might not have a practical relevance (e.g. coded targets can be used and only 3 GCP are necessary for georeferencing). Hence, without considering this time all technologies are similarly efficient.

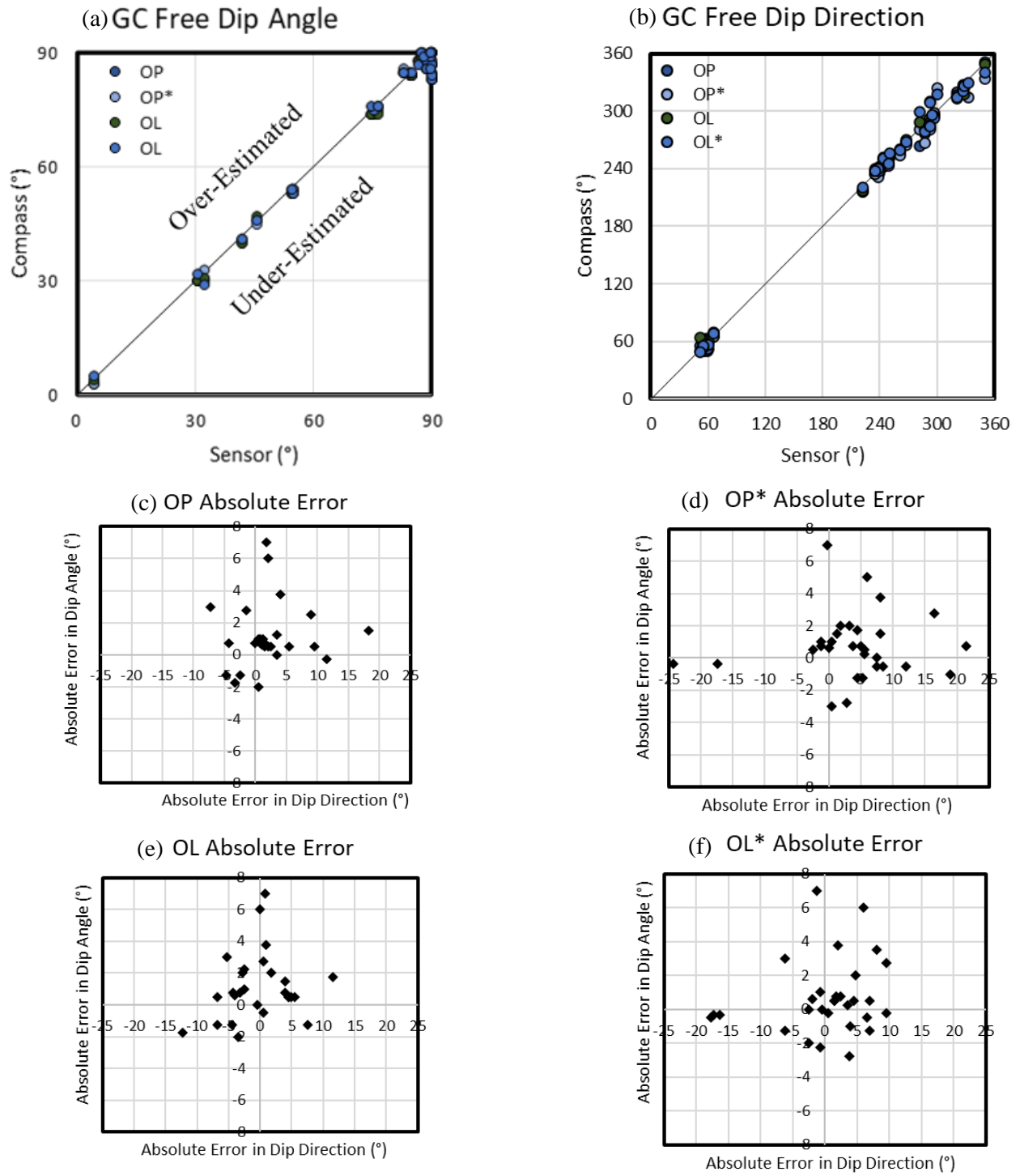


**Figure 16.** Typical results; example contact measurement results for the Oppo R9 phone with the GC free software.

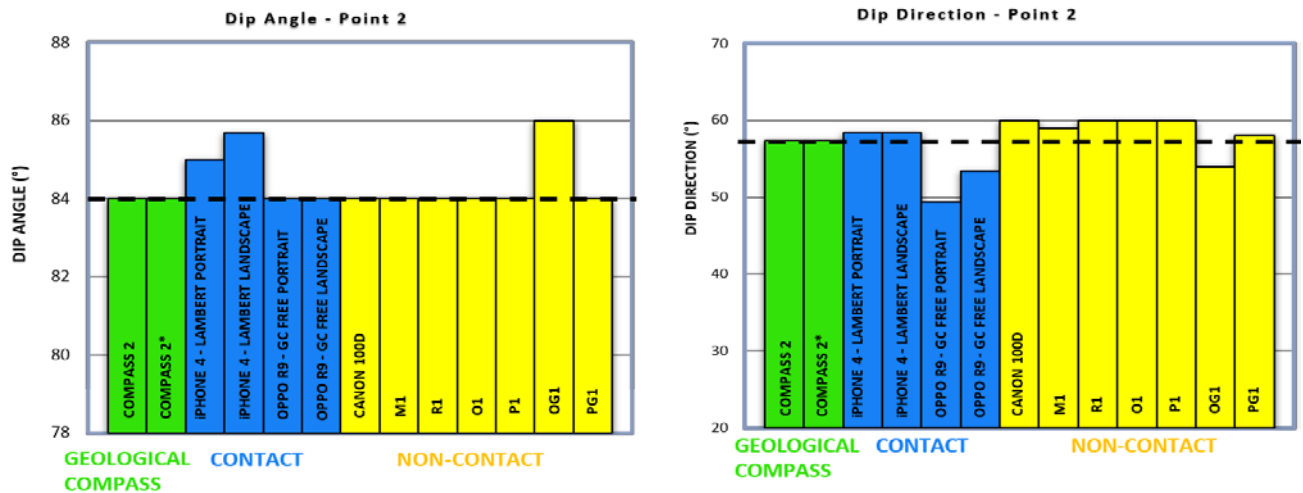
**Table 4** Summary of errors in measurements using the Oppo R9 phone with the GC free app.

Key	OP	OL	OP*	OL*	OP	OL	OP*	OL*
Error Percentile (°)	Angle				Direction			
$x \leq 1$	18	15	17	18	9	4	4	4
$1 > x \leq 3$	9	12	10	8	9	9	6	9
$3 > x \leq 5$	1	1	2	2	6	5	5	5
$5 > x \leq 10$	2	2	1	2	4	9	9	9
$x = 10+$	0	0	0	0	2	3	6	3
Sum	30	30	30	30	30	30	30	30

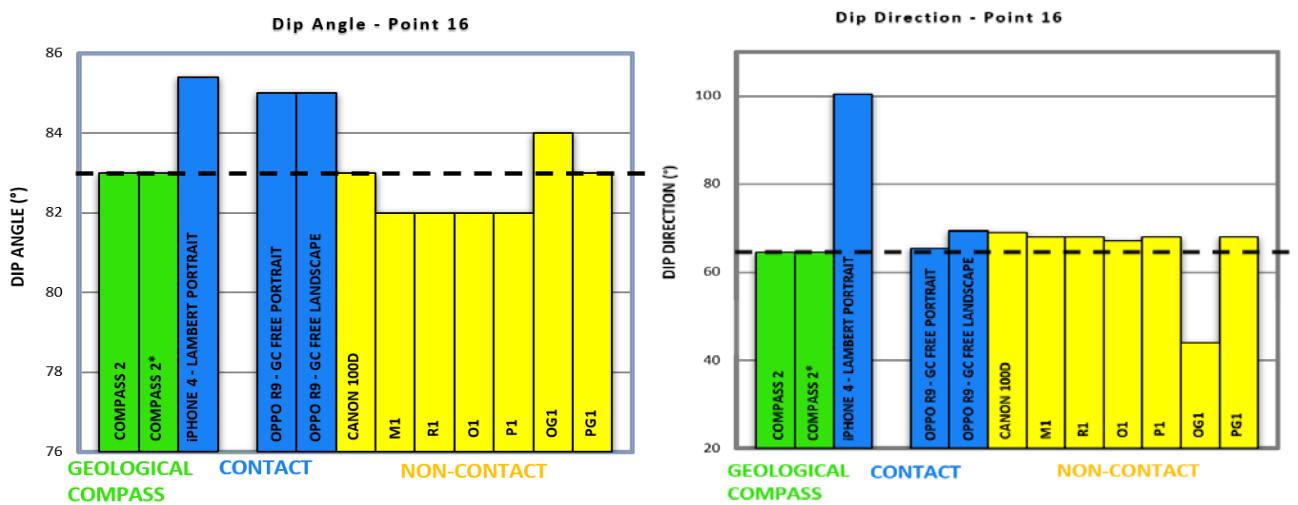
**Table 5** Summary of errors for the different technologies tested.

Sensor	Keys	Category	Dip	Occurrence of error (out of 30)					Time (h)	Sensor Cost (AUD)
				<1°	<3°	<5°	<10°	10°+		
iPhone 4 - Lambert	IP, IL, IP*, IL*	Contact	Angle	18	8	1	2	1	2.5	\$700
			Direction	3	5	4	5	13		
Oppo R9 - GC free	OP, OL, OP*, OL*	Contact	Angle	17	10	1	2	0	2.5	\$600
			Direction	5	8	5	8	4		
Canon 100D	C1	Non-Contact	Angle	18	8	2	2	0	6 <sup>+</sup>	\$900
			Direction	9	11	4	3	3		
Moto G5 Plus	M1	Non-Contact	Angle	18	9	0	2	1	6 <sup>+</sup>	\$400
			Direction	9	12	2	2	5		
Raspberry Pi	R1	Non-Contact	Angle	16	9	2	3	0	6.5 <sup>+</sup>	\$60
			Direction	8	11	4	2	5		
Oppo R9	O1	Non-Contact	Angle	16	10	2	2	0	6.5 <sup>+</sup>	\$600
			Direction	9	12	2	2	5		
Phantom 3 Pro	P1	Non-Contact	Angle	13	10	1	4	2	6 <sup>+</sup>	\$2000
			Direction	6	11	4	1	8		
Oppo R9 GPS	OG1	Non-Contact	Angle	12	12	3	2	1	3	\$600
			Direction	3	1	3	5	18		
Phantom 3 Pro GPS	PG1	Non-Contact	Angle	16	9	1	4	0	2	\$2000
			Direction	12	10	2	2	6		

<sup>+</sup> includes 4 hours of selecting/collimating GCP.



(a) Comparison of outcomes for Point 2 with the lowest variation of the chosen features.



(b) Comparison of outcomes for Point 16 with the highest variation of the chosen features. Note that landscape meurement of the iPhone could not been taken due to calibration issue.

**Figure 17.** Comparison of outcomes for Points 2 and 16, with the lowest and highest variation of the chosen features, respectively. The dashed line (reference) presents the measurement taken by the geological compass.

## 7. Conclusions

This paper presents a systematic comparison of measurements of geological features (i.e. dip and dip direction) taken by different technologies and sensors. Two different smartphones were used to take contact measurements by placing the device on the features. Images were collected using different sensors and different platforms including a low-cost camera module, two smartphones, an off-the-shelf UAV and a DSLR. The acquired image sets were processed using Agisoft Metashape to obtain virtual high-resolution 3D models. The 3D models were analysed in CloudCompare to derive measurements of the same features. All measurements were compared against measurements taken by a conventional geological compass.

From the results it can be seen that most of the methods were generally found to be acceptably reliable. Of the results from the smartphone applications, that of the iPhone 4 (an older generation) was more unreliable. It provided inaccurate dip direction due to the device constantly requiring calibration. Generally, the dip angle was approximated better than the dip direction for both devices tested. Further the results suggest that the error in the dip angle is not affected by whether the device is oriented in portrait or landscape on the face, or whether it is placed on a backing block, or directly against the rock. The error in dip direction is also unaffected by the use of a mounting block, but it does seem that the error is reduced when the device is oriented in landscape position.

All photogrammetric sensors tested performed relatively well. Generally, the measurements were more accurate for the dip angle than the dip direction. As expected, the highest resolution camera, the Canon 100D produced the most accurate measurements when compared to the geological compass. On average 90% of the points measured for the dip angle fell in the less than three degree error category. 70% of points measured for dip direction had less than three degree error. This trend was uniform across all photogrammetric models. It was also found that the measurements from the model built from the images taken with the Moto G5 had roughly the same degree of error as the one taken from the Canon 100D model yet the retail price is less than half the price. Even more impressive was the performance of the Raspberry Pi, being the cheapest sensor tested, with an 83% less than three degree error for dip angle and 66% less than three degree error for dip direction. The accuracy was slightly lower, but the cost is significantly different meaning the Raspberry Pi was a viable option. Furthermore, the GPS model produced from the Phantom UAV had 83% less than three degree error for dip angle and 73% less than three degree error for dip direction. This is a very promising results indicating that low-cost off-the-shelf UAVs might be suitable for geostructural mapping applications. The major advantage of such platforms is also the ease of use and the benefit of achieving vantage points which would not otherwise be possible.

Overall, there is not much difference between the different technologies, and certainly, the performance is not directly proportional to price. Both contact and non-contact technologies appear to be capable of giving

reliable measurements of dip and dip direction in most situations. There is no case to argue that contact technologies are more or less reliable than non-contact technologies. Hardware and software have advanced very rapidly over the last decade and have initiated a new era of 3D mapping. Proximity remote sensing methods provide added benefits such as keeping the user safe and providing more data in an automated way. Virtual models can be stored on devices for record keeping and there is no need to go back to take additional measurements. There is no doubt that these technologies will offer new and even better possibilities in the future at even lower cost.

## References

- [1] Clar, E., "A dual-circle geologist's and miner's compass for the measurement of areal and linear geological elements", *Separate print from the negotiations of the Federal Institute of Geology Vienna*, Vol. 4, 1954
- [2] Diggelen, F. V., Enge, P. "The world's first GPS MOOC and Worldwide Laboratory using Smartphones", *Proceedings of the 28<sup>th</sup> International Technical Meeting of The Satellite Division of the Institute of Navigation*, pp. 361–369, 2015
- [3] Allmendinger, R. W., Siron, C. R., Scott, Chelsea P. "Structural data collection with mobile devices: Accuracy, redundancy, and best practices", *Journal of Structural Geology*, 102, 98–112, 2017
- [4] Djuric, U., Dragana, P., Marjanovic, M., Kuzmic, P. "Portable Geotechnics – Using Android Smartphones and Tablets for Geotechnical Field Investigations", *Proceedings of the International Multidisciplinary Scientific GeoConference SGEM*, pp. 513–520, 2013
- [5] Farny, N. J. "Comparing Rock Discontinuity Measurements Using Geological Compass, Smartphone Application, and Laser Scanning Methods", *Environmental & Engineering Geoscience*, XXIII(2), pp. 97–111, 2017
- [6] Lee, S., Suh, J., Park, H. D. "Smart Compass-Clinometer: A smartphone application for easy and rapid geological site investigation", *Computers & Geoscience*, 61, pp. 32–42, 2013
- [7] Weng, Y-H., Sun, F-S., Grigsby, J. D. "GeoTools: An android phone application in geology", *Computers & Geosciences*, 44, pp. 24–30, 2012
- [8] Haneberg, W. "Using close range terrestrial digital photogrammetry for 3-D rock slope modeling and discontinuity mapping in the United States", *Bulletin of Engineering Geology and the Environment*, 67(4), pp. 457–469, 2008
- [9] Assali, P., Grussenmeyer, P., Villemin, T., Pollet, N., Viguier, F. "Surveying and modelling of rock discontinuities by terrestrial laser scanning and photogrammetry: Semi-automatic approaches for linear outcrop inspection", *Journal of Structural Geology*, 66, pp. 102–114, 2014
- [10] Smith, M. W., Carrivick, J. L., Quincey, D. J. "Structure from motion photogrammetry in physical geography", *Progress in Physical Geography*, 40(2), pp. 247–275, 2016
- [11] Thoeni, K., Giacomini, A., Murtagh, R. K., Knies, E. "A Comparison of Multi-view 3D Reconstruction of a Rock Wall using Several Cameras and a laser scanner", *The International Archives of the Photogrammetry, Remote Sensing and Spatial Information Sciences*, XL-5, pp. 573–580, 2014
- [12] Lato, M.J., Vöge, M. "Automated mapping of rock discontinuities in 3D LiDAR and photogrammetry models", *International Journal of Rock Mechanics and Mining Sciences*, 54, pp. 150–158, 2012
- [13] Sturzenegger, M., Stead, D. "Quantifying discontinuity orientation and persistence on high mountain rock slopes and large landslides using terrestrial remote sensing techniques", *Natural Hazards and Earth System Sciences*, 9, pp. 267–287, 2009
- [14] Thiele, S. T., Grose, L., Samsu, A., Micklethwaite, S., Vollgger, S. A., Cruden, A. R. "Rapid, semi-automatic fracture and contact mapping for point clouds, images and geophysical data", *Solid Earth*, 8, pp. 1241–1253, 2017
- [15] Westoby, M. J., Brasington, J., Glasser, N. F., Hambrey, M. J., Reynolds, J. M. "'Structure-from-Motion' photogrammetry: A low-cost, effective tool for geoscience applications", *Geomorphology*, 179, pp. 300–314, 2012

- [16] Aguera-Vega, F., Carvajal-Ramirez, F., Martinez-Carricondo, P., Sanchez-Hermosilla Lopez, J., Mesas-Carrascosa, F. J., Garcia-Ferrer, A., Perez-Porras, F. J. "Reconstruction of extreme topography from UAV structure from motion photogrammetry", *Measurement*, 121, pp. 127–138, 2018
- [17] Bemis, S. P., Micklethwaite, S., Turner, D., Bangash, H. A., James, M. R., Akcize, S., Thiele, S. "Ground-based and UAV-Based photogrammetry: A multi-scale, high-resolution mapping tool for Structural Geology and Paleoseismology", *Journal of Structural Geology*, 69, pp. 163–178, 2014
- [18] Kong, D., Saroglou, C., Wu, F., Sha, P., Li, B. "Development and application of UAV-SfM photogrammetry for quantitative characterization of rock mass discontinuities", *International Journal of Rock Mechanics and Mining Sciences*, 141, 104729, 2021
- [19] Thoeni, K., Guccione, D. E., Santise, M., Giacomini, A., Roncella, R., Forlani, G. "The potential of low-cost RPAS for multi-view reconstruction of sub-vertical rock faces", *The International Archives of the Photogrammetry, Remote Sensing and Spatial Information Sciences*, XLI-B5, pp. 909–916, 2016.
- [20] Tscharf, A., Rumpler, M., Fraundorfer, F., Mayer G., Bischof, B. "On the use of UAVs in mining and archaeology – geo-accurate 3D reconstruction using various platforms and terrestrial views", *ISPRS Annals of the Photogrammetry, Remote Sensing and Spatial Information Sciences*, II-1/W1, pp. 15–22, 2015
- [21] Santise, M., Thoeni, K., Roncella, R., Sloan, S. W., Giacomini, A. "Preliminary tests of a new low-cost photogrammetric system", *The International Archives of the Photogrammetry, Remote Sensing and Spatial Information Services*, XLII-2/W8, pp. 229–236, 2017
- [22] Tannant, D. D. "Review of Photogrammetry-Based Techniques for Characterization and Hazard Assessment of Rock Faces", *International Journal of Georesources and Environment*, 1(2), pp. 76–87, 2015.
- [23] Thoeni, K., Santise, M., Guccione, D. E., Fityus, S., Roncella, R., Giacomini, A. "Use of low-cost terrestrial and aerial imaging sensors for geotechnical applications", *Australian Geomechanics Journal*, 53(3), pp. 101–122, 2018
- [24] Agisoft Metashape (2021). Version 1.7.2. Available at: <http://www.agisoft.com> [Accessed: 17 May 2021]
- [25] CloudCompare (2021). Version 2.11.3 Available at: <http://www.danielgm.net/cc> [Accessed: 17 May 2021]